CHAPTER ONE

Markov Modeling of Ion Channels: Implications for Understanding Disease

Angelika Lampert[*,†], **Alon Korngreen**[‡,§]

[*]Institute of Physiology and Pathophysiology, Friedrich-Alexander Universität Erlangen-Nuremberg, Erlangen, Germany
[†]Institute of Physiology, RWTH Aachen University, Aachen, Germany
[‡]The Mina and Everard Goodman Faculty of Life Sciences, Bar-Ilan University, Ramat-Gan, Israel
[§]The Gonda Brain Center, Bar-Ilan University, Ramat-Gan, Israel

Contents

Abstract

Ion channels are the bridge between the biochemical and electrical domains of our life. These membrane crossing proteins use the electric energy stored in transmembrane ion gradients, which are produced by biochemical activity to generate ionic currents. Each ion channel can be imagined as a small power plant similar to a hydroelectric power station, in which potential energy is converted into electric current. This current drives basically all physiological mechanisms of our body. It is clear that a functional blueprint of these amazing cellular power plants is essential for understanding the principle of all aspects of physiology, particularly neurophysiology. The golden path toward this blueprint starts with the biophysical investigation of ion channel activity and continues through detailed numerical modeling of these channels that will eventually lead to a full system-level description of cellular and organ physiology. Here, we discuss the first two stages of this process focusing on voltage-gated channels, particularly the voltage-gated sodium channel which is neurologically and pathologically important.

Progress in Molecular Biology and Translational Science, Volume 123
ISSN 1877-1173
http://dx.doi.org/10.1016/B978-0-12-397897-4.00009-7

We first detail the correlations between the known structure of the channel and its activity and describe some pathologies. We then provide a hands-on description of Markov modeling for voltage-gated channels. These two sections of the chapter highlight the dichotomy between the vast amounts of electrophysiological data available on voltage-gated channels and the relatively meager number of physiologically relevant models for these channels.

1. WHY DO WE NEED MODELING?

1.1. Ion channel diseases: Mutations focus attention on ion channels

Human cells possess an extensive variety of ion channels. Depending on its type, a single cell may express several hundred genes for different types of ion channels.[1] Recent years have seen a tremendous advance in our understanding of their individual roles as well as of their physiological interplay. Their specific fine-tuned function is so delicate that malfunction of a single-channel subtype, due to mutation or dysregulation, may result in serious and sometimes even life-threatening diseases.[2–4]

In this chapter, we focus on voltage-gated ion channels. Of the vast number of these channels, we shall focus on voltage-gated sodium channels (Nav), as these are responsible for the upstroke of the neuronal action potential and display complex gating mechanisms. They are also involved in a broad spectrum of diseases[5]; two of the most intensely investigated disorders based on Nav modulation are epilepsy and pain. In both cases, a single-point mutation leads to severe clinical symptoms.[6,7] The resulting biophysical changes are frequently not easily understood in the context of neuronal excitability and phenotype.

1.2. Structure and function of voltage-gated sodium channels

The α subunit of voltage-gated sodium channels is sufficient to form a functional channel. It contains four domains (DI–DIV) that are connected by intracellular linkers. Each domain consists of six transmembrane helices (Fig. 1.1A; Ref. 9). The S5 and S6 segments of each domain come together to form the pore (Fig. 1.1B and C), which is gated by voltage-dependent conformational changes. Positive charges in S4 sense changes in membrane potential and move within the voltage-sensing domain (VSD), formed by S1–S4. This movement is transferred to the pore by the S4–S5 linkers,

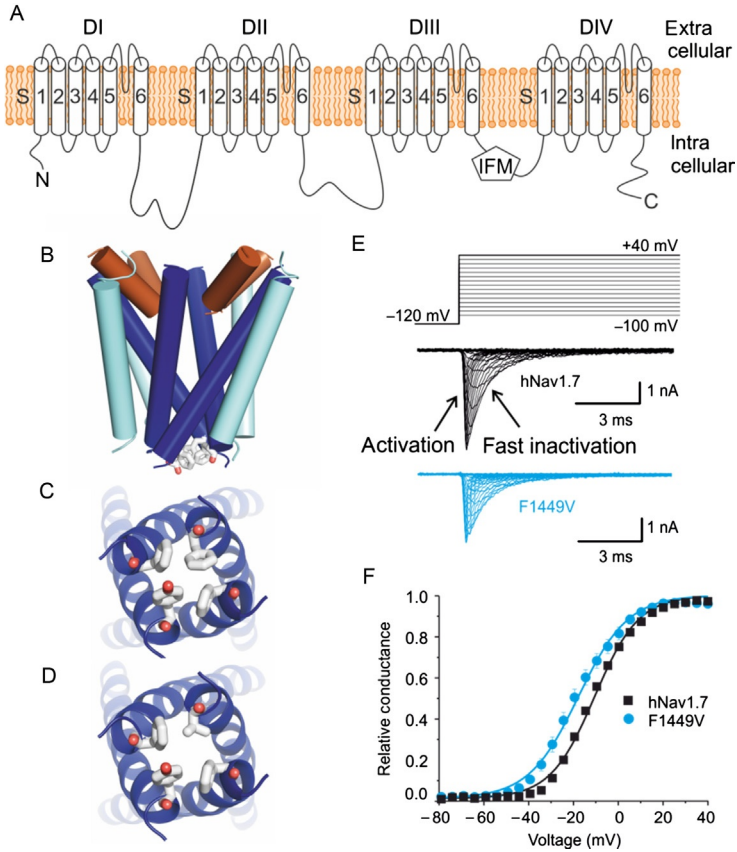

Figure 1.1 (A) 2D structure of mammalian voltage-gated sodium channels (α subunit) in the cell membrane. The four domains (DI–DIV) containing six segments each are connected by an intracellular linker. The IFM motif marks the inactivation particle. (B) Side view of the pore region of a homology model of Nav1.7. The pore is formed by the S5 and S6 segments of each domain (voltage-sensing domains are omitted for better visibility). (C) A ring of hydrophobic amino acids is situated at the intracellular face, which may act as the activation gate. (D) When mutated in the erythromelalgia mutation p.F1449V, the hydrophobic interaction may be interrupted and activation made easier. (E) Current recordings from transfected HEK cells expressing either hNav1.7 WT (black traces) or the erythromelalgia mutation p.F1449V (blue traces). Using the indicated voltage protocol, fast opening and closing voltage-gated sodium currents were recorded. (F) Conductance-voltage relation for hNav1.7 WT and its p.F1449V mutation show that the erythromelalgia mutation shifts the voltage-dependence of hNav1.7 to more hyperpolarized potentials. *(B)–(F) Adapted from Lampert* et al.[8]

and by their elevation toward the outside of the cell the S6 segments splay apart and open the permeation pathway.

Not all domains contain the same amount of gating charges (four in DI, five in DII, six in DIII, and eight in DIV) and, probably due to varying stiffness of the S6, their voltage sensitivity differs. In the skeletal muscle subtype Nav1.4, DII is quickest to move upon change in membrane potential, directly followed by DIII, whereas DI and especially DIV lag behind.[10] This complex gating behavior allows several nonconducting conformational states to manifest. Activation of more than one VSD increases the channel's probability of being open and may be reflected by several nonconducting states in Markov models.

The channel inactivates within milliseconds after opening: a hydrophobic motif on the DIII–DIV linker, the IFM motif/inactivation particle, binds to its receptor site at the cytosolic side of the pore and obliterates the permeation pathway. This inactivated state is nonconducting and needs to be reflected in stochastic models, as the channels must recover from inactivation at hyperpolarized potentials for a certain time before they can open again. Channels may not only be inactivated from the activated, conducting state, but also from the closed states, adding to the complexity that must be reflected by a computational model aiming to faithfully model the channel's gating behavior.

In addition to fast inactivation, sodium channels show a slow inactivated state which is occurring at a much longer time scale. Channels enter this nonconducting state within seconds at elevated potentials and recover from it within a similar time range. Slow inactivation is physiologically relevant when there are changes in resting membrane potential, for example, due to altered synaptic input or additional ion conductances in the cell membrane. It is relevant for dendritic integration[11] and affected by some disease causing mutations (such as small fiber neuropathy (SFN) or myopathy[12,13]). Some drugs target slow inactivation[14] and are used with some success for the treatment of epilepsy or diabetes-induced pain.

To date nine sodium channel genes have been identified in the human body (Scn1a to Scn6a, Scn8a to Scn11a), coding for the α subunits Nav1.1 to Nav1.9.[15] In the CNS, generally Nav1.1, 2, 3, and 6 are expressed, whereas the PNS additionally displays Nav1.7, 1.8, and 1.9. The latter two are slightly slower in their gating, as is subtype Nav1.5 (specific to the heart). Skeletal muscle mainly expresses Nav1.4. All sodium channel subtypes can be associated with up to two modulatory β subunits, for which four genes have so far been identified, Scn1b–Scn4b. The two disease entities that

we focus on in this chapter can be caused by mutations in Nav1.7 (pain) and Nav1.1 (epilepsy).

Excitability of a neuron is shaped both by its ion channels and its morphology. Unfortunately, cell morphology often imposes severe limitations on recording from certain parts of the cell. It is technically possible to record from the cell soma, but it is incomparably harder to gain data from dendrites or axons. Therefore, most of our electrophysiological data are collected from the cell soma. We assume that excitability in the soma is comparable to that in other parts of the cell. It is feasible to create a Markov model of several conductances based on data from the cell soma or heterologously expressed channels (see below). *In silico* it is easy to place these conductances, for example, on the axon or nerve ending, and thereby assess the impact of gating changes, such as those induced by disease-causing mutations.

1.3. Epilepsy and pain can be induced by sodium channel mutations

Epilepsy and pain are both syndromes based on an increased neuronal excitability. The need for integrative methods that help us understand the role of channel alteration in causing this hyperexcitability is underlined by the >600 mutations found in Nav1.1 which are linked with mild to very severe forms of epilepsy. Many of these mutations are loss-of-function mutations (LOFs); Dravet Syndrome, for example, is a catastrophic early life epilepsy disorder, which is usually refractory to treatment and results in intellectual decline. This syndrome is caused mainly by LOFs. How can LOFs result in hyperexcitability[6]? Nav1.1 is expressed at high levels on inhibitory interneurons and loss of excitability here could result in decreased network inhibition.[16] On the other hand, interaction with other sodium channel subtypes, variation in expression and channel distribution may also play an important role. These are questions that are hard to address experimentally but can be investigated using computer models.

Four inherited pain syndromes are linked to mutations in Nav1.7, which is mainly expressed in sensory neurons of the dorsal root ganglia (DRGs). Complete loss of function of Nav1.7 leads to the absence of pain—affected patients mutilate themselves and have a reduced life expectance.[7] Gain-of-function mutations (GOFs), however, lead to the severe pain disorders erythromelagia (IEM), paroxysmal extreme pain disorder (PEPD) and SFN.

IEM patients suffer attacks of excruciating pain accompanied by reddening of the skin in their extremities triggered by warmth or mild exercise.

The patients describe the attacks, for example, ". . . as if hot lava is poured on the skin." Most of the patients do not profit from pharmaceutical treatment. Most IEM mutations render the channels more voltage sensitive, resulting in an opening of the channels at lower potentials (e.g., the mutation F1449V; Fig. 1.1F). This shift of the voltage dependence of activation eases action potential formation by normally subthreshold stimulation and is therefore likely to produce pain. In contrast, many other IEM mutations enhance slow inactivation, which may alleviate pain, as fewer channels are available.[17]

PEPD mutations, on the other hand, hamper fast inactivation, thereby producing persistent sodium currents. Most of the mutations display a slowed current decay indicating that the rate constant for the transition from the open to the inactivated state is slowed. This leads to prolonged opening of the channel, which favors the occurrence of resurgent currents[18]: an endogenous open channel blocker, most likely the c-terminal end of the β4 subunit,[19] occludes the open pore at positive potentials. As the blocking particle is positively charged, it is removed from the pore upon repolarization, and sodium current may flow until the inactivation particle finally binds. This resurgent current is most prominent in the cerebellum[20] where it supports high frequency firing. It is mostly carried by Nav1.6,[21] but other subtypes are also capable of producing resurgent currents.[22] It was recently shown that PEPD mutations also enhance the normally barely detectable resurgent currents of Nav1.7.[23] Slowing current decay increases the likelihood of binding of the endogenous blocker and thus potentially enhancing resurgent currents. This feature is only observed in PEPD mutations and not in mutated channels associated with IEM.[24] Thus, biophysically, PEPD is very different from IEM. The clinical presentation is also markedly different: attacks of PEPD triggered by cold or mechanical stimulation affect very young children within their first year of life. The pain is located in proximal body parts and is accompanied by a harlequin-type skin reddening.

To test for mutation-induced changes in excitability, PEPD or IEM mutations were transfected in rodent DRG neurons. Not surprisingly, both increased action potential firing and lowered their threshold (e.g., Ref. 25). What causes the remarkable difference in their clinical presentation? So far, we can only speculate and more detailed investigations, including cell morphology, temperature, age-dependent regulations, and possible changes in ion concentrations close to the cell membrane, may improve our understanding. It would be most helpful to have a valid computer model to help produce hypotheses that can be assessed experimentally (see Table 1.1 and Fig. 1.2).

Table 1.1 Electrophysiological recording of transfected rodent DRGs (rDRGs)

Advantages	Disadvantages
rDRGs are neurons with all necessary components (e.g., Kvs, Cavs, subunits, etc.,)	rDRGs are not human. Therefore all cellular components are based on rodent genetics
rDRGs are similar to human nociceptors	In whole-cell patch clamp •the intracellular ion concentrations are clamped •regulatory molecules are dialyzed out of the cell
The somata of rDRGs are easily accessible	The soma of the cell was investigated, but nociception occurs in the nerve endings, which are very hard to patch

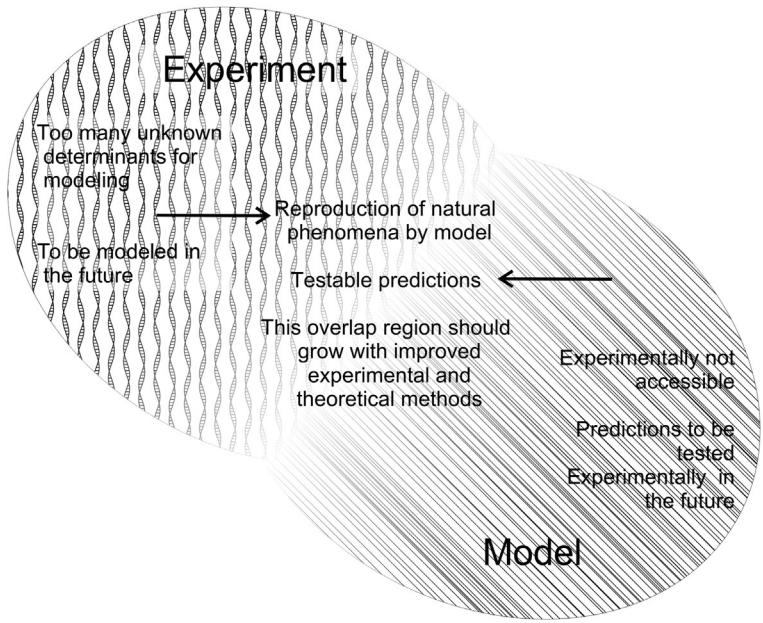

Figure 1.2 Scheme illustrating the applicability of *in vitro* experiments (left), computational models (right), and their potential interaction (middle).

The third pain disorder caused by mutations in Nav1.7, SFN, typically occurs later in life and leads to a degeneration of the peripheral nerve endings.[26] Patients report intense pain and symptoms of the autonomous nervous system and only occasionally reddening of the skin. SFN patients thus describe symptoms that can also be found in IEM or PEPD, although to a

different extent and at a different age. Biophysically, the major effect of SFN mutations is impairment of slow inactivation, in contrast to the IEM mutations that often enhance this gating characteristic. For example, the I228M mutation does not display any major gating change other than an enhanced slow inactivation. Still, it increases excitability when transected into DRG neurons,[27] suggesting that impaired slow inactivation is capable of inducing disease.

Why do the mutations causing IEM mainly enhance slow inactivation, whereas those inducing SFN reduce it? Many possible *in vitro* experiments have already provided valuable insights, but this obvious difference remains hard to explain. *In silico* it is relatively easy to model the impact of mutant-induced slow inactivation in various disease conditions. Therefore, a reliable model of the sodium conductance would be most helpful.

The following questions may be addressed using an *in silico* modeling approach:

- A neuron expresses a large variety of ion channels, including different sodium channel subtypes and other conductances, such as Kv and Cav. How do disease-causing mutations affect their interplay?
- Different types of neurons display different sets of ion channels. How does the cellular background affect the impact of a mutation and could this explain variations in clinical presentation (e.g., why do PEPD and SFN patients have symptoms of the autonomous nervous system, while IEM patients do not)?
- What is the effect of cell morphology on neuronal excitability altered by a mutation?
- How can different gating changes induce the same clinical symptoms?
- Some patients present a genetic mosaic for their mutation—is the gene load important for cellular excitability?
- Why and how does temperature trigger attacks of hyperexcitability?
- How does ion accumulation/depletion close to the membrane affect excitability?

1.4. How can Markov models help understand the pathophysiology of channelopathies?

In physiological experiments, it is possible to determine the biophysical gating changes induced by single-point mutations, as outlined above. These parameters may be used to create a Markov model (see below), which not only helps us model the whole cellular excitability but also to understand

Table 1.2 Computational modeling of channelopathies

Advantages	Disadvantages
All conductances may be derived from human data	All conductances used for the model are results from experiments that are affected by experimental constraints
Conductances may be varied and adjusted, modeling different gene loads and neuronal cell types	There may be components necessary for cellular excitability that we do not yet know
Gating changes may be modeled in isolation	
Ion concentrations may be modeled and their change due to cellular activity may be monitored	
Cell morphology is taken into account	
Temperature can be implied	All predictions need to be tested experimentally to validate the model

occupancy of gating states (Table 1.2 and Fig. 1.2). These Markov models need to be validated by predicting gating changes that can be experimentally tested.

Markov models have only been rarely used for modeling channelopathies to date, probably because Markov models are assumed to make sense only when single-channel data are used. Nevertheless, there are already some examples, mostly models of Nav1.5 involved in arrhythmias, such as long QT syndrome.[28–31] A Markov model of an epilepsy mutation faithfully modeled persistent currents and predicted that inactivation of SCN1A open-state consists of two-steps, an initial gate closure followed by an additional mechanism to stabilize the inactivated state.[32] Interference with this mechanism may induce the epileptic symptoms of the Nav1.1 mutation investigated in this study.

2. MARKOV MODELS BUILT BASED ON WHOLE-CELL PATCH-CLAMP DATA

Having shown the need for valid computational models of voltage-gated ion conductances, we now focus on how these models are best generated. Ion channels are large transmembrane proteins constructed from a very large number of covalent bonds. From a purely chemical point of view,

each bond contributes not only to the structure of the molecule but also to its dynamics. Each bond vibrates at a typical spring frequency that can be described using chemical kinetics. Thus, the "true" representation of the structural and dynamic properties of the ion channel can be defined as a set of equations roughly equaling the number of bonds in the protein. For a voltage-gated channel, we also need to add the sensitivities of some amino acid residues to the external electric field and the interactions of the protein with water, ions, and membrane lipids. All these equations must be implemented in a computer model and then time-intensive calculations must be performed to determine the activity of the channel. These molecular dynamics simulations, while of crucial importance to understanding the relationship between structure and function, are too slow and way too detailed to be helpful to the physiologist or even to the garden variety biophysicist.

We now show an approach that is a possible solution to this problem. All functional models are, by definition, phenomenological. Therefore, we will treat them according to standard formulations of chemical kinetics. First, let us consider the nature of the reaction. In mammals, ion channels (and all cellular reactions for that matter) operate at ~37 °C. Ion channels can move reversibly between the open and closed states. Thus, according to thermodynamical laws this reaction has low free energy and is close to equilibrium. Changes in extrinsic parameters, such as membrane potential or the concentration of a ligand, perturb the channel away from equilibrium. Similar to many systems at equilibrium, the channel responds to this perturbation by an apparently exponential relaxation. Formally, the simplest reaction of this kind can be written using the following chemical notation. This is the simplest "Markov model," just two links in the chain.

$$C \underset{k_{-1}}{\overset{k_1}{\rightleftharpoons}} O \tag{1.1}$$

$$\begin{aligned} I &= \bar{g} O (V - E) \\ \frac{\mathrm{d}C}{\mathrm{d}t} &= -k_1 C + k_{-1} O \\ \frac{\mathrm{d}O}{\mathrm{d}t} &= k_1 C - k_{-1} O \end{aligned} \tag{1.2}$$

Where O denotes the open state, C the closed state, k is a kinetic rate constant having units of 1/s, V is the membrane potential, I is the ionic current, E is the Nernst potential, and $\bar{g}$ is the maximal conductance. Here, we denote the forward reaction by a positive subscript and the reverse reaction

by a negative subscript. Many Markov models of ion channels use a different notation with numbering related to the states and not to the transition. According to this alternative, we have two states and the rate constants will be k_{12} and k_{21}. We find both numbering systems equally confusing. Remembering that according to the principle of mass conservation $C+O=1$, it is possible to write the differential equation for the open state as

$$\frac{\mathrm{d}O}{\mathrm{d}t}=k_1(1-O)-k_{-1}O \tag{1.3}$$

From here, it can be simply shown that under steady-state conditions that $O_{\mathrm{inf}}=k_1/(k_1+k_{-1})$ and that the relaxation time constant of the reaction is $\tau=1/(k_1+k_{-1})$.

This general description of the system holds for every simple one-stage chemical or biological reaction that is close to equilibrium. Here, we focus on voltage-gated channels. Thus the rate constants should be a function of the membrane potential in the general exponential form:

$$k=A\mathrm{e}^{BV}$$

where V is the membrane potential in volts and the rate constants are in 1/s. Thus, A has units of 1/s and B units of 1/V. Let us start with two simple and opposite rate constants:

$$k_1=10\mathrm{e}^{50V};\;\; k_{-1}=10\mathrm{e}^{-50V} \tag{1.4}$$

First, let us look at the steady-state condition:

$$O_{\mathrm{inf}}=\frac{10\mathrm{e}^{50V}}{10\mathrm{e}^{50V}+10\mathrm{e}^{-50V}}=\frac{1}{1+\mathrm{e}^{-100V}}$$

Here, we can easily see the link between the rate constants and the classical Boltzmann curve that is so typical for the description of the voltage dependence of voltage-gated channels. For graphical convenience, we plotted k_1, k_{-1} (Fig. 1.3A), the open probability at steady state (O_{inf}) (Fig. 1.3B), and the time constant (Fig. 1.3C) all as a function of the membrane potential. Several insights can be extracted from Fig. 1.3 and from the above equation. First, it is instructive to note the direction and trend of the rate constants. The voltage dependence of the channel is a direct function of the voltage dependence of the rate constants. At hyperpolarized values of the membrane potential, $k_{-1}\gg k_1$, drawing the reaction toward the closed state. The opposite picture emerges at depolarized potentials where

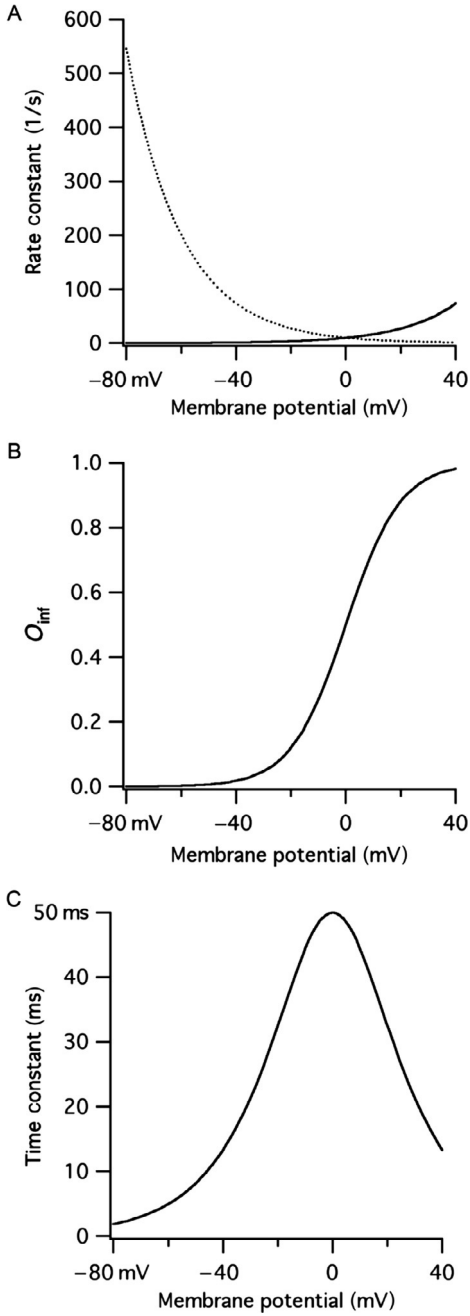

Figure 1.3 (A) The rate functions plotted as a function of the membrane potential of the kinetic scheme shown in Eq. (1.1). The forward rate constant is shown by the solid line and the backward rate constant by the dashed line. (B) Steady-state activation curve for this kinetic model. (C) Activation time constant for this model.

$k_{-1} \ll k_1$ and the reaction is drawn to the open state. When $k_1 = k_{-1}$ it is simple to see from Eq. (1.4) that $O_{\text{inf}} = 1/2$. This value of the membrane potential is often referred to by experimentalists as the potential of half activation or $V_{1/2}$. For the simple case, we are currently discussing this is also the potential at which the maximal value of τ can be observed (Fig. 1.3C). This correlation between $V_{1/2}$ and the maximal time constant holds true for many models and can serve as a simple sanity check of the integrity of one's model.

Now let us look at a slightly more complex model, one with two closed states and one open state. We write the differential equations explicitly here and will then display the same system as a matrix.

$$C_1 \underset{k_{-1}}{\overset{k_1}{\rightleftharpoons}} C_2 \underset{k_{-2}}{\overset{k_2}{\rightleftharpoons}} O \tag{1.5}$$

$$\begin{aligned} \frac{dC_1}{dt} &= -k_1 C_1 + k_{-1} C_2 \\ \frac{dC_2}{dt} &= k_1 C_1 - k_{-1} C_2 - k_2 C_2 + k_{-2} O \\ \frac{dO}{dt} &= k_2 C_2 - k_{-2} O \end{aligned} \tag{1.6}$$

From this simple model it is possible to grasp the general rule describing the kinetics of a given transition. The rate of change is given as the sum of the rates entering that state minus the sum of the rates leaving it. What is also clear from this set of equations is that it is the product of a matrix of the rate constants with the vector of the states (Eq. 1.7a). This matrix is known as the Q matrix and is comprehensively described in depth in several publications.[33,34] It has been extensively used for simulating and analyzing single-channel activity. The reader will therefore find that most sources refer to the states in terms of probabilities. This is strictly correct, however, for our current discussion of whole-cell currents we can, *quasi* correctly, treat the states as a continuous level of occupancy.

When constructing the Q matrix two simple rules must be applied:

$q_{i,i} = -\sum$(transition rates leading away from the state i)

$q_{i,j} =$ (transition rates from state i to state j)

Thus the Q matrix for Eq. (1.5) appears as

$$Q = \begin{Bmatrix} -k_1 & k_1 & 0 \\ k_{-1} & -(k_2 + k_1) & k_2 \\ 0 & k_{-2} & -k_{-2} \end{Bmatrix} \tag{1.7}$$

With the equivalent of Eq. (1.6) in matrix form

$$\begin{Bmatrix} dC_1/dt \\ dC_2/dt \\ dO/dt \end{Bmatrix} = \begin{Bmatrix} -k_1 & k_1 & 0 \\ k_{-1} & -(k_2 + k_{-1}) & k_2 \\ 0 & k_{-2} & -k_{-2} \end{Bmatrix} \begin{Bmatrix} C_1 \\ C_2 \\ O \end{Bmatrix} \tag{1.7a}$$

When the rate constants are not dependent on the membrane potential, it is possible to solve this matrix analytically to obtain the relaxation time constants of the channel.[33,34] When the rate constants are voltage dependent, it is usually not possible to provide an analytical solution. However, once the Q matrix is known, it is relatively simple to solve the system using Matlab or Mathematica. There are also several freely available software packages that are specifically designed for simulating Markov models of ion channels. We will discuss these packages later.

The third example we mention briefly can be expressed by the following kinetic scheme:

$$C \underset{k_{-1}}{\overset{k_1}{\rightleftharpoons}} O \underset{k_2}{\overset{k_{-2}}{\rightleftharpoons}} I, \tag{1.8}$$

where I represents an inactivated nonconducting state. We will not describe this scheme in depth, as it is less applicable to physiological cases. This model, once fully inactivated, must change to the open state in order to return to the closed state. Such channel activity has been observed but is rare and is usually considered only as part of a larger model. Another important point for the construction of a model with inactivation is the inversion of the transition rates between the open and inactivated state, as opposed to those between the closed and open states (cf. Eq. 1.5). This is required for the proper setting of the inactivated state. It is possible to use the following cyclic kinetic scheme to overcome the need to change to the open state on the way from inactivated to closed.

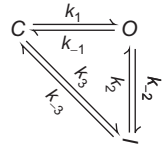

(1.9)

In this model, given the correct setting of the rate constants, the channel moves from open to inactivated and from there to closed, without generating an unwanted current by reversing from inactivated back to the open state. The Q matrix for this model is

$$Q = \begin{Bmatrix} -(k_1 + k_3) & k_1 & k_3 \\ k_{-1} & -(k_{-2} + k_{-1}) & k_{-2} \\ k_{-3} & k_2 & -(k_2 + k_{-3}) \end{Bmatrix} \tag{1.10}$$

Another important issue must be discussed when considering cyclic mechanisms. It is clear that the scheme depicted by Eq. (1.9) contains two opposing reaction cycles, one on the outside and one on the inside of the scheme. Again, considering this as a chemical reaction, one can see that even at equilibrium there is continuous cycling of material in opposite directions. Clearly, in order for the reaction to balance, the total rate of the external cycle should be equal to that of the internal one

$$k_1 k_{-2} k_{-3} = k_{-1} k_2 k_3 \tag{1.11}$$

Leading to

$$k_{-3} = \frac{k_{-1} k_2 k_3}{k_1 k_{-2}} \tag{1.12}$$

Thus, for cyclic mechanisms one of the rate constants is not independent but should be expressed as a function of the other constants reducing the system's degrees of freedom by one. This is called the principle of microscopic reversibility.[35] These four examples (Eqs. 1.1–1.12) can be viewed as basic building blocks that can be used to construct almost any functionally relevant Markov chain model of voltage-gated ion channels.

3. PRACTICAL CONSIDERATIONS FOR FITTING MODELS TO DATA

Having drawn the skeleton of the model, we must now select values for the rate constants. This is the difficult part. Considering again the kinetic scheme displayed in Eq. (1.5), we have four rate constants, each described by two parameters (Eq. 1.4) leading to eight free parameters. This number of free parameters explodes when more states are added to the model. The nonlinearity of the system impedes tuning and even eight free parameters are exceedingly hard to tune by hand.

Yet, before we address the tuning options, we survey the types of rate constants used in modeling voltage-gated ion channels. The rate constants we discussed previously (Eq. 1.4) can be derived from general kinetic theory.[36] However, several other equations have been used to describe rate constants in Markov models of voltage-gated channels. In an attempt to shift

the activation curve along the membrane potential axis, rate constants have been often described by a modified version of Eq. (1.4):

$$k = A\mathrm{e}^{b(V-c)} \tag{1.13}$$

However, this formulation is misleading as can be demonstrated by simple algebra.

$$A\mathrm{e}^{b(V-c)} = A\mathrm{e}^{bV-bc} = \left(A\mathrm{e}^{-bc}\right)\mathrm{e}^{bV} \tag{1.14}$$

The term in the parentheses is constant and, therefore, does not convey any shift of the activation curve along the membrane potential axis. It is easy to see that Eq. (1.13) is just an unnecessarily complex form of Eq. (1.4). The exponential rate constant can be extended using thermodynamic rationalization to include higher terms of voltage dependence.[37] These rate constants can account for voltage-dependent transitions that are rate limited while retaining a low number of states in the model:

$$k = A\mathrm{e}^{bV+cV^2} \tag{1.15}$$

Forsaking the attempt to use thermodynamically based rate constants, a popular way of calculating rate constants is via the Boltzmann equation.

$$k = \frac{a}{1+\mathrm{e}^{-b(c-V)}} \tag{1.16}$$

It is important to note that using Eq. (1.15) or Eq. (1.16) to describe the transition rates in Eq. (1.5) increases the number of free parameters for this model to 12. Here lies one of the major problems in constructing models for ion channels and particularly for voltage-gated ion channels. Even for a three-state model, the number of free parameters ranges from 8 to 12 and possibly even more. With such a high number of free parameters that require adjusting it is almost impossible to tune these models by hand.

One way to reduce this parameter space is to assume that some states are dependent on others. For example, writing the Markov chain model for the Hodgkin–Huxley potassium channel we obtain the following scheme:

$$C \underset{\beta}{\overset{4\alpha}{\rightleftharpoons}} C \underset{2\beta}{\overset{3\alpha}{\rightleftharpoons}} C \underset{3\beta}{\overset{2\alpha}{\rightleftharpoons}} C \underset{4\beta}{\overset{\alpha}{\rightleftharpoons}} O \tag{1.17}$$

Here, we have only two rate constants that are factored between transitions to reach the original Hodgkin–Huxley formalism after solving the Q matrix.

3.1. Fitting experimental data to Markov models

Another facet of ion channel modeling is fitting the model to a set of experimental results. This requires selecting the right data set, the right cost function and the appropriate fitting algorithm. In this review, we do not address the issue of single-channel recording and analysis, as most physiologically relevant kinetic analyses of voltage-gated ion channels in recent decades have been performed on ensemble currents obtained from whole-cell or excised patch recordings. Furthermore, almost all investigations so far have applied the analysis paradigm established by Hodgkin and Huxley.[38]

At the practical level this celebrated analysis methodology proceeds in several simple steps. First, one must construct steady-state activation curves of the investigated conductance (and inactivation curves if required). These curves are then used to estimate the number of activation gates in the Hodgkin–Huxley-like model that best fits the investigated conductance. Armed with the number of gates, one can now fit the current traces, one by one, to the model and secure the activation (and/or inactivation) time constants. This procedure has not changed considerably for some decades and we have often found that the original papers by Hodgkin and Huxley[38–41] are a better source of information than modern papers.

Still, this analysis procedure may introduce severe errors in the estimation of the kinetic constants of the investigated channel, especially if the activation and inactivation time constants are not sufficiently different.[42] The source of the problem is the separate (or disjoint, see Ref. 42) analysis of the steady-state and kinetic properties of the current. This severe error source can be overcome by simultaneous curve fitting of a Hodgkin–Huxley-like model to a data set including current traces recorded at several voltages.[42,43] Direct fitting of a model to a set of current traces was also recently introduced into the single-channel analysis software QUB,[44] allowing the fitting of Markov chain models to whole-cell currents. In contrast to the conventional method, this approach to data analysis and model fitting has been named global curve fitting or the full trace method.[42,43]

It is important to remember that fitting a full model to a set of data dramatically increases the number of free parameters. To complicate the problem, standard curve-fitting algorithms (such as, e.g., the simplex and gradient descent algorithms) tend to settle into a local minimum when dealing with many parameters.[45] Thus, to verify that the solution obtained is not a local minimum, it is important to select initial values that are sufficiently close to the global minimum. Alternatively, instead of guessing a set of initial values

that may lead the minimization algorithm to a local minimum, it is possible to apply stochastic minimization algorithms to search a predefined parameter space.

Several popular stochastic minimization tools such as genetic algorithms[46] and simulated annealing[47] have been successfully applied to many problems of nonlinear curve fitting in biology. These algorithms usually perform tens to hundreds of thousands of iterations to find the global minimum. Their advantage over the more commonly used gradient descent algorithms is that genetic algorithms do not require an initial guess of the parameters.[42–44] With a large enough data set it is possible to arrive at the global minimum even from a random starting point.[48–51] This advantage of genetic algorithms is important as, given wrong starting parameters, gradient descent algorithms may arrive at a local minimum and mistakenly provide a model with "good" fitting parameters. However, the genetic algorithm method is not infallible, there may be a random combination of parameters that defy it. But our results show that a useable and functionally significant ion channel model describing whole-cell currents can be produced using a genetic algorithm with a data set containing a "complete" whole-cell activation of the channel as its input.[49,52]

We have encountered computational exhaustion due to the complexity of the models and the amount of electrophysiological data. To solve this computational bottleneck, we converted our optimization algorithm for work on a graphical processing unit using NVIDIA's CUDA. Parallelizing the process on a Fermi graphic computing engine from NVIDIA increased the speed $\sim 180\times$ over an application running on an 80 node Linux cluster, considerably reducing simulation times. This application allows users to optimize models for ion channel kinetics on a single, inexpensive, desktop "super computer," greatly reducing the time and cost of building models relevant to neuronal physiology.[53,54]

4. CONCLUSION AND OUTLOOK

In this chapter, we deliberately split the discussion of ion channel function into two separate and only partially overlapping sections. We first elaborated on some of the advances in the study of the function and pathology of voltage-gated sodium channels. We then detailed the basic terminology and considerations behind building a successful Markov model for a voltage-gated channel. The dichotomy between these two parts of the chapter highlights the current state of the field of ion channel modeling that is

graphically displayed in Fig. 1.2. There is a vast body of experiments from structure-function studies in many expression systems. However, the conversion of these studies to physiologically relevant kinetic models lags far behind. Several current trends may assist in closing this gap. First, computing power has increased in vast leaps during the last two decades and is now accessible to almost any researcher of ion channels. Secondly, while only 10 years ago fitting a model to a set of data required mastodonic parallel computers, through the low cost and availability of multicore desktop computers and the amazing advances in using graphic and DSP cards for parallel computing, the power of supercomputing will reach the investigator's desktop, if not today, then most definitely in the very near future. We predict that, given this surge in new and exciting hardware, we will soon see user friendly software that will enable any electrophysiologist to easily fit large quantities of voltage-clamp data to functional Markov models of ion channels in the comfort of his/her lab. This will be a major step toward better understanding the role of ion channels in cell function in health and disease.

ACKNOWLEDGMENTS

This work was supported by a joint grant from the German-Israeli Foundation to A. K. and A. L. (#1091-27.1/2010).

REFERENCES

1. Gabashvili I, Sokolowski BA, Morton C, Giersch AS. Ion Channel Gene Expression in the Inner Ear. *J Assoc Res Otolaryngol*. 2007;8:305–328.
2. Ashcroft F. *Ion Channels and Disease: Channelopathies*. Boston, MA: Academic; 2000.
3. Ashcroft FM. From molecule to malady. *Nature*. 2006;440:440–447.
4. Nilius B. A Special Issue on channelopathies. *Pflugers Arch*. 2010;460:221–222.
5. Eijkelkamp N, Linley JE, Baker MD, et al. Neurological perspectives on voltage-gated sodium channels. *Brain*. 2012;135:2585–2612.
6. Escayg A, Goldin AL. Sodium channel SCN1A and epilepsy: mutations and mechanisms. *Epilepsia*. 2010;51:1650–1658.
7. Lampert A, O'Reilly A, Reeh P, Leffler A. Sodium channelopathies and pain. *Pflugers Arch*. 2010;460:249–263.
8. Lampert A, O'Reilly AO, Dib-Hajj SD, Tyrrell L, Wallace BA, Waxman SG. A pore-blocking hydrophobic motif at the cytoplasmic aperture of the closed-state Nav1.7 channel is disrupted by the erythromelalgia-associated F1449V mutation. *J Biol Chem*. 2008;283:24118–24127.
9. Catterall WA. Voltage-gated sodium channels at 60: structure, function and pathophysiology. *J Physiol*. 2012;590:2577–2589.
10. Chanda B, Bezanilla F. Tracking voltage-dependent conformational changes in skeletal muscle sodium channel during activation. *J Gen Physiol*. 2002;120:629–645.
11. Mickus T, Jung H, Spruston N. Properties of slow, cumulative sodium channel inactivation in rat hippocampal CA1 pyramidal neurons. *Biophys J*. 1999;76:846–860.
12. Lossin C, Nam TS, Shahangian S, et al. Altered fast and slow inactivation of the N440K Nav1.4 mutant in a periodic paralysis syndrome. *Neurology*. 2012;79:1033–1040.

13. Waxman SG. Painful Na-channelopathies: an expanding universe. *Trends Mol Med*. 2013;19:406–409.
14. Errington AC, Stoehr T, Heers C, Lees G. The investigational anticonvulsant lacosamide selectively enhances slow inactivation of voltage-gated sodium channels. *Mol Pharmacol*. 2007;73:157–169. http://dx.doi.org/10.1124/mol.107.039867.
15. Catterall WA, Goldin AL, Waxman SG. International Union of Pharmacology. XLVII. Nomenclature and structure-function relationships of voltage-gated sodium channels. *Pharmacol Rev*. 2005;57:397–409.
16. Ogiwara I, Miyamoto H, Morita N, et al. Nav1.1 localizes to axons of parvalbumin-positive inhibitory interneurons: a circuit basis for epileptic seizures in mice carrying an Scn1a gene mutation. *J Neurosci*. 2007;27:5903–5914.
17. Sheets PL, Jackson 2nd JO, Waxman SG, Dib-Hajj SD, Cummins TR. A Nav1.7 channel mutation associated with hereditary erythromelalgia contributes to neuronal hyperexcitability and displays reduced lidocaine sensitivity. *J Physiol*. 2007;581:1019–1031.
18. Bean BP. The molecular machinery of resurgent sodium current revealed. *Neuron*. 2005;45:185–187.
19. Grieco TM, Malhotra JD, Chen C, Isom LL, Raman IM. Open-channel block by the cytoplasmic tail of sodium channel beta4 as a mechanism for resurgent sodium current. *Neuron*. 2005;45:233–244.
20. Raman IM, Bean BP. Resurgent sodium current and action potential formation in dissociated cerebellar Purkinje neurons. *J Neurosci*. 1997;17:4517–4526.
21. Raman IM, Sprunger LK, Meisler MH, Bean BP. Altered subthreshold sodium currents and disrupted firing patterns in Purkinje neurons of Scn8a mutant mice. *Neuron*. 1997;19:881–891.
22. Rush AM, Dib-Hajj SD, Waxman SG. Electrophysiological properties of two axonal sodium channels, Nav1.2 and Nav1.6, expressed in mouse spinal sensory neurones. *J Physiol*. 2005;564:803–815.
23. Jarecki BW, Piekarz AD, Jackson 2nd JO, Cummins TR. Human voltage-gated sodium channel mutations that cause inherited neuronal and muscle channelopathies increase resurgent sodium currents. *J Clin Invest*. 2010;120:369–378.
24. Theile JW, Jarecki BW, Piekarz AD, Cummins TR. Nav1.7 mutations associated with paroxysmal extreme pain disorder, but not erythromelalgia, enhance Navbeta4 peptide-mediated resurgent sodium currents. *J Physiol*. 2011;589:597–608.
25. Dib-Hajj SD, Yang Y, Black JA, Waxman SG. The Na(V)1.7 sodium channel: from molecule to man. *Nat Rev Neurosci*. 2013;14:49–62.
26. Hoeijmakers JG, Faber CG, Lauria G, Merkies IS, Waxman SG. Small-fibre neuropathies—advances in diagnosis, pathophysiology and management. *Nat Rev Neurol*. 2012;8:369–379.
27. Estacion M, Han C, Choi JS, et al. Intra- and interfamily phenotypic diversity in pain syndromes associated with a gain-of-function variant of NaV1.7. *Mol Pain*. 2011;7:92.
28. Bankston JR, Sampson KJ, Kateriya S, et al. A novel LQT-3 mutation disrupts an inactivation gate complex with distinct rate-dependent phenotypic consequences. *Channels (Austin)*. 2007;1:273–280.
29. Ruan Y, Denegri M, Liu N, et al. Trafficking defects and gating abnormalities of a novel SCN5A mutation question gene-specific therapy in long QT syndrome type 3. *Circ Res*. 2010;106:1374–1383.
30. Vecchietti S, Rivolta I, Severi S, Napolitano C, Priori SG, Cavalcanti S. Computer simulation of wild-type and mutant human cardiac Na+ current. *Med Biol Eng Comput*. 2006;44:35–44.
31. Vecchietti S, Grandi E, Severi S, et al. In silico assessment of Y1795C and Y1795H SCN5A mutations: implication for inherited arrhythmogenic syndromes. *Am J Physiol Heart Circ Physiol*. 2007;292:H56–H65.

32. Kahlig KM, Misra SN, George Jr AL. Impaired Inactivation Gate Stabilization Predicts Increased Persistent Current for an Epilepsy-Associated SCN1A Mutation. *J Neurosci*. 2006;26:10958–10966.
33. Colquhoun D, Hawkes AG. The principles of the stochastic interpretation if ion-channel mechanisms. In: Sakmann B, Neher E, eds. *Single-Channel Recording*. New York, NY: Plenum Press; 1995:397–482.
34. Colquhoun D, Sigworh JF. Fitting and staistical analysis of single channels records. In: Sakmann B, Neher E, eds. *Single-Channel Recording*. New York, NY: Plenum Press; 1995:483–589.
35. Colquhoun D, Dowsland KA, Beato M, Plested AJ. How to impose microscopic reversibility in complex reaction mechanisms. *Biophys J*. 2004;86:3510–3518.
36. Johnson FH, Eyring H, Stover GJ. *The Theory of Rate Processes in Biology and Medicine*. New York, NY: Wiley; 1974.
37. Destexhe A, Huguenard JR. Nonlinear thermodynamic models of voltage-dependent currents. *J Comput Neurosci*. 2000;9:259–270.
38. Hodgkin AL, Huxley AF. A quantitative description of membrane current and its application to conduction and excitation in nerve. *J Physiol*. 1952;117:500–544.
39. Hodgkin AL, Huxley AF. The components of membrane conductance in the giant axon of Loligo. *J Physiol*. 1952;116:473–496.
40. Hodgkin AL, Huxley AF. The dual effect of membrane potential on sodium conductance in the giant axon of Loligo. *J Physiol*. 1952;116:497–506.
41. Hodgkin AL, Huxley AF. Currents carried by sodium and potassium ions through the membrane of the giant axon of Loligo. *J Physiol*. 1952;116:449–472.
42. Willms AR, Baro DJ, Harris-Warrick RM, Guckenheimer J. An improved parameter estimation method for Hodgkin-Huxley models. *J Comput Neurosci*. 1999;6:145–168.
43. Willms AR. NEUROFIT: software for fitting Hodgkin-Huxley models to voltage-clamp data. *J Neurosci Methods*. 2002;121:139–150.
44. Milescu LS, Akk G, Sachs F. Maximum likelihood estimation of ion channel kinetics from macroscopic currents. *Biophys J*. 2005;88:2494–2515.
45. Press WH, Teukolsky SA, Vetterling WT, Flannery BP. *Numerical Recipes in C, the Art of Scientific Computing*. 2nd ed. Cambridge: Cambridge University Press; 1992.
46. Mitchell M. *An Introduction to Genetic Algorithms*. Cambridge, MA: MIT Press; 1996.
47. Kirkpatrick S, Gelatt CD, Vecchi MP. Optimization by simulated annealing. *Science*. 1983;220:671–680.
48. Gurkiewicz M, Korngreen A. Recording, analysis, and function of dendritic voltage-gated channels. *Pflugers Arch*. 2006;453:283–292.
49. Gurkiewicz M, Korngreen A. A numerical approach to ion channel modelling using whole-cell voltage-clamp recordings and a genetic algorithm. *PLoS Comput Biol*. 2007;3:e169.
50. Keren N, Peled N, Korngreen A. Constraining compartmental models using multiple voltage recordings and genetic algorithms. *J Neurophysiol*. 2005;94:3730–3742.
51. Keren N, Bar-Yehuda D, Korngreen A. Experimentally guided modelling of dendritic excitability in rat neocortical pyramidal neurones. *J Physiol*. 2009;587:1413–1437.
52. Gurkiewicz M, Korngreen A, Waxman SG, Lampert A. Kinetic modeling of Nav1.7 provides insight into erythromelalgia-associated F1449V mutation. *J Neurophysiol*. 2011;105:1546–1557.
53. Ben-Shalom R, Liberman G, Korngreen A. Accelerating compartmental modeling on a graphical processing unit. *Front Neuroinform*. 2013;7:4.
54. Ben-Shalom R, Aviv A, Razon B, Korngreen A. Optimizing ion channel models using a parallel genetic algorithm on graphical processors. *J Neurosci Methods*. 2012;206:183–194.